Attosecond-resolution quantum dynamics calculations for atoms and molecules in strong laser fields

Rui-Feng Lu and Pei-Yu Zhang
State Key Laboratory of Molecular Reaction Dynamics, Dalian Institute of Chemical Physics, Chinese Academy of Sciences, Dalian, 116023, China
and Graduate School of the Chinese Academy of Sciences, Beijing 10039, China

Ke-Li Han*
State Key Laboratory of Molecular Reaction Dynamics, Dalian Institute of Chemical Physics, Chinese Academy of Sciences, Dalian 116023, China
and Virtual Laboratory for Computational Chemistry, CNIC, CAS, China
(Received 4 December 2007; revised manuscript received 28 February 2008; published 2 June 2008)

A parallel quantum electron and nuclei wave packet computer code, LZH-DICP, has been developed to study laser-atom-molecule interaction in the nonperturbative regime with attosecond resolution. The nonlinear phenomena occurring in that regime can be studied with the code in a rigorous way by numerically solving the time-dependent Schrödinger equation of electrons and nuclei. Time propagation of the wave functions is performed using a split-operator approach, and based on a sine discrete variable representation. Photoelectron spectra for hydrogen and kinetic-energy spectra for molecular hydrogen ion in linearly polarized laser fields are calculated using a flux operator scheme, which testifies to the validity and the high efficiency of LZH-DICP.

DOI: 10.1103/PhysRevE.77.066701 PACS number(s): 05.10.−a, 33.80.−b

I. INTRODUCTION

Despite several years of study, the interaction of intense laser pulses with atoms and molecules remains a very attractive problem, with the continuing development of new light sources, particularly short pulses of increasing intensity [1,2]. In the areas of strong lasers, a substantial effort is being dedicated to producing subfemtosecond (that is, attosecond) pulses and real-time observation of the motion of electrons for experimentalists and theorists alike. The progress in attosecond science and technology has been reviewed very recently [3], and a lot of ultrafast dynamics phenomena can be probed by the attosecond resolution method. From a theoretical point of view, investigating the nonlinear phenomena such as above-threshold dissociation (ATD), above-threshold ionization (ATI), high-order harmonic generation (HHG), and dynamics stabilization in the nonperturbative regime relies on exact numerical solutions of the time-dependent Schrödinger equation (TDSE) on recently available supercomputers. Actually, numerous theoretical researches, not only for atoms but also for molecules, have been carried out up to date.

In addition to classical interpretation [4], various quantum models and numerical methods have been proposed and studied. Some have assumed the Born-Oppenheimer (BO) approximation [5–11], especially for molecules, while the multielectronic-state model has been commonly adopted [12,13]. Other calculations include the correlation between electron and nuclear motions (i.e., without the BO approximation) [14–22], however, it should be noted that simplified non-BO models have also been taken, for example, in the works of Hu *et al.* [23] and Lein [24]. Generally, soft Coulomb potential, as well as the reasonable choice of the coordinate to reduce the dimensionality, could make the problem to be more manageable. As for the time propagator, the Crank-Nicholson (CN) method of different forms has been introduced [25]. Although the CN scheme has the advantage of unconditional stability and the alternating-direction implicit (ADI) method [17] even cures the computational inefficiency for multidimensional cases, computing the matrix inversion is still time consuming. Moreover, the ADI method is found to be not rigorously unitary [26]. In a grid based approach, fast Fourier transform (FFT) is also a good candidate, but it would still require a relatively large number of grid points. In principle, the wave functions can be expanded in a proper set of orthogonal basis functions such as Bessel-Fourier series, Legendre polynomials, *B* splines, spherical harmonics, Tri-Morse functions, etc.

In this paper, we introduce a useful split-operator approach coupled to a discrete variable representation (DVR). Sine basis functions are used to define the DVR for the radial part; we therefore denote this method as the sine-DVR method [27], which has been extensively verified in reactive scattering and energy transfer processes [28]. Direct comparison is made between the sine-DVR method and CN finite-difference method, which demonstrated that the former is superior to the latter. Hence, the method will provide a high efficient technique to the quantum dynamics study of atoms and molecules in intense laser fields at an attosecond time scale. Moreover, with the help of a parallel instrument, the implementation of our computer code LZH-DICP can be significantly speeded up.

The organization is given as follows. In Sec. II, we begin with the introduction of sine-DVR, and comparison between the two methods mentioned above is also shown; then we outline the theory for atom and diatomic molecule cases, respectively. In Sec. III, we apply this scheme for extracting

*Corresponding author; klhan@dicp.ac.cn

TABLE I. The spatial step, time step (both in atomic units), and the total CPU time corresponding to sine-DVR and CN schemes on a 3.2 GHz Pentium 4D. Three examples are presented (see text). Note that the results of examples II and III are obtained by LZH-DICP without the parallelization (d: days; h: hours; m: minutes; s: seconds).

	Ex. I Photodissociation for HCl			Ex. II For H atom			Ex. III 1D model for H_2^+			
	ΔR	Δt	T_{CPU}	Δr	Δt	T_{CPU}	ΔR	Δz	Δt_e	T_{CPU}
sine-DVR	0.05	10	2 s	0.2	0.1	2 h 47 m 29 s	0.1	0.4	0.2	5 h 2 m 33 s
CN	0.01	2	3 m 28 s	0.15	0.05	3 d 7 h 20 m 6 s	0.05	0.2	0.1	8 d 12 h 11 m 57 s

the dynamical information of both hydrogen atom and molecular hydrogen ion in linearly polarized fields, and the results together with discussions are also presented. Section IV is devoted to some conclusions and perspectives.

II. THEORY

A. Sine-DVR and CN schemes

Although the DVR algorithm originated from bound states calculations has so far been mainly applied in both the time-independent and time-dependent context for solving bound and scattering problems, it should be equally useful in current quantum wave packet calculations in external fields. We employ the sine basis functions to define a DVR for the translational coordinate R, which was described in Ref. [27],

$$\langle R_i|n\rangle = \sqrt{\frac{2}{L}}\sin(n\pi R_i'/L) = \sqrt{\frac{2}{L}}\sin\left(\frac{in\pi}{N+1}\right), \tag{1}$$

where $L=R_{\max}-R_{\min}$, $R_i'=R_i-R_{\min}=i\Delta R$, $i=1,2,\ldots,N$, and $\Delta R=L/(N+1)$. The corresponding DVR basis $|\bar{R}_i\rangle$ is defined as

$$\langle \bar{R}_i|n\rangle = \sqrt{\Delta R}\langle R_i|n\rangle, \tag{2}$$

and the transformation between $|\bar{R}_i\rangle$ and $|n\rangle$ is orthogonal. The expansion of the wave function in sine basis functions has the main advantage over others, that is, this basis is the eigenfunction of the second-order differential kinetic energy operator, and the eigenvalue can be straightforwardly obtained. The time-dependent wave function is advanced using the standard second-order split-operator method

$$\psi(t+\delta t) = e^{-iT\delta t/2}e^{-iV\delta t}e^{-iT\delta t/2}\psi(t) + O(\delta t^3), \tag{3}$$

where T is the kinetic energy operator, and V is the interaction potential, taking all the potential energy of the system plus a purely imaginary term to produce an absorbing boundary. Unless stated otherwise, atomic units are used throughout the whole paper.

Different types of CN split operators have been reported [25,26]; for the sake of comparison to Eq. (3), we choose one taking the form

$$e^{-iH\delta t} \approx \left[1+i\frac{\delta t}{4}T\right]^{-1}\left[1-i\frac{\delta t}{4}T\right] \times e^{-iV\delta t}\left[1+i\frac{\delta t}{4}T\right]^{-1}\left[1-i\frac{\delta t}{4}T\right]. \tag{4}$$

To check the efficiency of both methods, test computations are performed for the photodissociation of HCl molecule; the condition is the same as that of Ref. [29]. The properties we examined are the absorption spectrum as well as the final wave function. Table I lists some parameters for this example (I) corresponding to sine-DVR and CN schemes and the total CPU time on a 3.4 GHz Pentium 4D. Obviously, in order to get convergence, the CN scheme needs smaller grid and time steps, and hence leads to more CPU time. As is well known, the inversion of matrices of the CN scheme is another time-consuming factor, so we could conclude that it is inferior to the sine-DVR scheme.

B. Model for atoms

In the single-active-electron and dipole approximations, the TDSE for the hydrogen atom or the single ionization of multielectron atoms is

$$i\frac{\partial}{\partial t}\psi(\mathbf{r},t) = [H_0(\mathbf{r}) + H_{\mathrm{int}}(\mathbf{r},t)]\psi(\mathbf{r},t), \tag{5}$$

the H_0 term is the atomic Hamiltonian

$$H_0(\mathbf{r}) = T + V = -\frac{1}{2}\nabla^2 + V(\mathbf{r}), \tag{6}$$

where $V(\mathbf{r})$ is the effective Coulomb potential. The H_{int} part of the Hamiltonian accounts for the laser-atom interaction

$$H_{\mathrm{int}}(\mathbf{r},t) = \mathbf{r}\cdot\mathbf{E}(t)\sin\,\omega t, \tag{7}$$

with the laser frequency of ω and the electric field envelope of $\mathbf{E}(t)$.

The treatment of the three-dimensional problem can proceed either in spherical coordinates or in Cartesian coordinates. The former is usually adopted for convenience, and the electronic wave function can therefore be expanded as

$$\psi(\mathbf{r},t) = \sum_{l=0}^{\infty}\frac{1}{r}\chi_l(r,t)Y_l^0(\theta), \tag{8}$$

where only spherical harmonics with $m=0$ have been introduced for simplicity. With the wave function in this expres-

sion, the TDSE can be solved by direct integration in two dimensionalities, or by leading to a set of coupled partial differential equations [5].

Explicitly, the coupled equations are

$$i\frac{\partial}{\partial t}\chi_i(r,t) = \mathbf{H}\chi_i(r,t), \quad i = 1,2,\ldots,l+1. \tag{9}$$

The diagonal matrix element of $\mathbf{H}$ is

$$H_{ii} = -\frac{1}{2}\frac{\partial^2}{\partial r^2} + V(r) + \frac{i(i-1)}{2r^2}, \quad i = 1,2,\ldots,l+1, \tag{10}$$

while the off-diagonal matrix elements

$$H_{ij} = \begin{cases} c_i^+ rE(t)\sin\omega t & \text{for } j = i+1, \\ c_i^- rE(t)\sin\omega t & \text{for } j = i-1, \\ 0 & \text{else} \end{cases} \tag{11}$$

and $c_i^{\pm}$ are the coupling constants related to Clebsch-Gordan coefficients, having the form

$$c_i^+ = c_{i+1}^- = \sqrt{\frac{i^2}{(2i-1)(2i+1)}}, \quad i = 1,2,\ldots,l+1. \tag{12}$$

The evolution of the electronic wave function in our calculation is performed utilizing an extended split operator which is similar to that for the nonadiabatic reactive and energy transfer systems [28]. Note that the sine-DVR scheme could be conveniently applied to the radial wave function $\chi(r,t)$. The observable values thus can be extracted from the final wave functions, such as harmonic generation, photoelectron energy spectra, angular distributions, and so on.

C. Model for molecules

For the diatomic molecule systems, in dipole approximation in the length gauge just as the aforementioned atom case, when we consider the linearly polarized nonrelativistic laser field along with the molecular axis, the Hamiltonian reads

$$\begin{aligned} H = &-\frac{1}{2\mu_N}\frac{\partial^2}{\partial R^2} + \frac{Z_a Z_b}{R} + \alpha RE(t)\sin\omega t \\ &+ \frac{1}{2}\sum_{i=1}^{N}\sum_{\substack{j=1 \\ (i\neq j)}}^{N}(i\neq j)\frac{1}{|\mathbf{r}_i - \mathbf{r}_j|} \\ &+ \sum_{i=1}^{N}\left[-\frac{1}{2\mu_e}\nabla_i^2 - \frac{Z_a}{|\mathbf{r}_i - R_a|} - \frac{Z_b}{|\mathbf{r}_j - R_a|}\right. \\ &\left. + \beta\mathbf{r}_i\cdot\mathbf{E}(t)\sin\omega t\right], \end{aligned} \tag{13}$$

where $\alpha = \frac{m_a - m_b}{m_a + m_b}$ and $\beta = \frac{m_a + m_b + 2}{m_a + m_b + 1}$. In this expression, note that it is often very useful to explore the behavior of a proton that lies along one axis of electronic coordinate, $R_a = \frac{m_a}{m_a + m_b}R$ and $R_b = \frac{m_b}{m_a + m_b}R$ are the positions for the atoms of the diatomic molecule, R is the internuclear distance, and $\mathbf{r}_i$ is measured with respect to the center-of-mass of the nuclei. $\mu_N = \frac{m_a m_b}{m_a + m_b}$ and $\mu_e = \frac{m_a + m_b}{m_a + m_b + 1}$ are the reduced masses of nuclei and electrons, respectively. Cartesian (x,y,z) or cylindrical (ρ,z) coordinates should be reasonably chosen, and together with the softcore Coulomb potential in terms of different situations. Practically, the case for $N > 2$ in Eq. (13) is beyond our quantum wave packet calculations. For the many-electron systems, it is well known that the time-dependent density-functional theory (TDDFT) which relies on the Kohn-Sham equations provides a genuine computational resort [30,31].

To further economize on computation time, we arrange the time evolution operator to take advantage of the disparity in the time scales of the nuclear and electronic motion; the resulting operator is

$$e^{-iH\delta t} \approx e^{-iT_R\delta t/2}\{U_e^{\mathrm{SPO}}(\delta t/M)\}^M e^{-iT_R\delta t/2}, \tag{14}$$

where

$$U_e^{\mathrm{SPO}}(\Delta t) = e^{-iT_e\Delta t/2}e^{-iV\Delta t}e^{-iT_e\Delta t/2} \tag{15}$$

represents the electronic part, T_R and T_e denote the nuclear and electronic kinetic-energy operators, respectively, and V subsumes all interactions and external potentials. We can estimate the ratio M to be $\sqrt{\mu_N/\mu_e}$; testing shows $M \approx 10$ is appropriate [22].

In fact, in addition to the item with respect to variant R, the sine-DVR scheme could be easily applied to the items relative to x,y,z in Cartesian coordinate. The items $\frac{\partial^2}{\partial\rho^2}$ and $\frac{\partial^2}{\partial z^2}$ in cylindrical coordinate can also be performed directly with the sine-DVR scheme, nevertheless, splitting of the item $\frac{1}{\rho}\frac{\partial}{\partial\rho}$ is so difficult that it can be customarily treated by the CN scheme.

III. RESULTS

For all of the calculations reported in this section, the quantum wave packet computer code LZH-DICP was employed, in which the sine-DVR scheme has been encoded. The initial wave packet can be constructed either by integrating the TDSE in imaginary time in the absence of the field with an initial guess, or by diagonalizing the field-free (discretized) Hamiltonian; the former has been chosen for both the below tests.

Figure 1 indicates the calculated photoelectron spectra from different methods for hydrogen atom in a linearly polarized fields; the laser parameters are $I = 1.7\times10^{14}$ W/cm^2, $\omega = 0.2$ a.u. for a 14-cycle pulse with a linear turn-on and turn-off of two cycles (example II). The corresponding result from the window operator method in Ref. [5] is also shown in Fig. 1. The propagation was performed with thirteen partial waves on a numerical grid which extends up to 400 with a spacing of $\Delta r = 0.2$, and the time interval $\Delta t = 0.1$ (2.4 as). Both radial and angular mask functions were used to avoid reflections from boundaries. Here we propose a flux operator method for the spectral analysis of wave functions. The energy distribution of the ionized electron can be obtained by calculating the flux at a fixed surface $r = r_{\mathrm{ion}}$ [28], which is

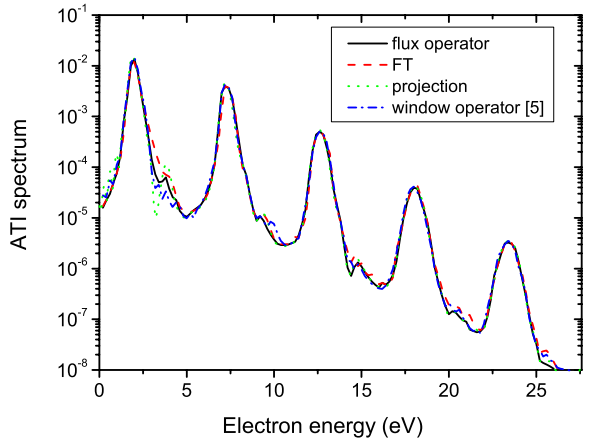

FIG. 1. (Color online) The calculated photoelectron spectrum (i.e., ATI spectrum) for hydrogen atom using different methods: (a) flux operator (black, solid), (b) FT (red, dashed), (c) projection (green, dotted), and (d) window operator from Ref. [5] (blue, dash-dotted). The laser parameters are $I=1.7\times10^{14}$ W/cm^2, $\omega=0.2$ a.u. for a 14-cycle pulse with a linear turn-on and turn-off of 2 cycles.

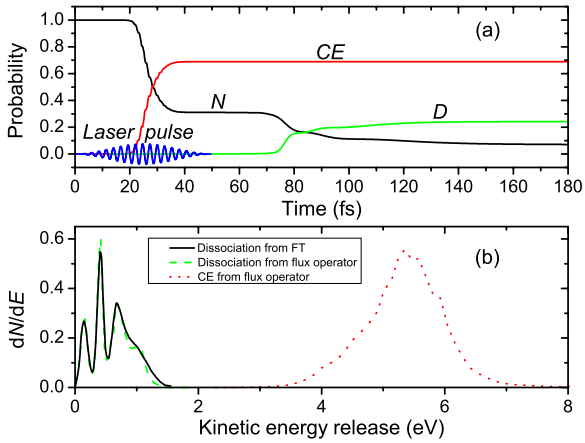

FIG. 2. (Color online) Fragmentation of H_2^+ ($v=3$) in a 25-fs 800-nm laser pulse of intensity $I=2.0\times10^{14}$ W/cm^2. (a) Time-dependent norm (N) and probabilities for Coulomb explosion (CE) and dissociation (D). (b) Kinetic-energy spectra for dissociation (from flux operator: black and solid line; from FT: green and dashed line) and ionization (i.e., CE channel from flux operator: red and dotted line).

$$S(E)=\mathrm{Im}\left[\langle\psi(E)|\delta(r-r_{\mathrm{ion}})\frac{\partial}{\partial r}|\psi(E)\rangle\right], \tag{16}$$

where

$$\psi(E)=(2\pi)^{-1/2}\int_0^\infty e^{iEt}\psi(t)dt. \tag{17}$$

The well-defined ATI spectrum is composed of a set of peaks separated by the energy of one laser photon, showing an overall exponential decrease in intensities with energies. Note that the ATI spectrum can also have been calculated from different methods: (a) a Fourier transformation (FT) to momentum space, (b) projection, and (c) the window operator [5]. The comparison between them shown in Fig. 1 demonstrates that the flux operator method is apparently able to solve the spectrum as others by adjusting the proper parameters such as the position for flux analysis, the size of the grid space, etc. Physically, it could be termed as another type of "virtual detector" which is brought forward because of the analogy to an experimental situation [32].

In terms of the test of molecular hydrogen ion (example III), the soft Coulomb potential is given by

$$V(R,z)=\frac{1}{R}-\frac{1}{\sqrt{(z-R/2)^2+1}}-\frac{1}{\sqrt{(z+R/2)^2+1}}, \tag{18}$$

resulting in a reduced one-dimensional (1D) model. The time evolution and the nuclear kinetic-energy spectra (KES) for H_2^+ ($v=3$) interacting with a 25-fs 800-nm laser pulse of intensity $I=2.0\times10^{14}$ W/cm^2 are illustrated in Fig. 2. The grid is defined by $0<R\leq30$ and $-45\leq z\leq45$ with the spatial step $\Delta R=0.1$ and $\Delta z=0.4$, and the time step for electron Δt_e is 0.2 (4.8 as). Absorbing regions extend over the last 50 grid points both on the outer R and z boundaries, thus the absorbing position R_s is chosen to be 25, and z_s is also 25. The norm of the total wave function is

$$N(t)=\int_0^{R_s}dR\int_{-z_s}^{z_s}dz|\psi(R,z,t)|^2, \tag{19}$$

and the probabilities for dissociation and ionization are defined as

$$P^d(t)=\int_0^t dt'\int_{-z_s}^{z_s}dz\,j(R_s,z,t'), \tag{20}$$

$$P^i(t)=\int_0^t dt'\int_0^{R_s}dR j(R,z_s,t'), \tag{21}$$

where

$$\mathbf{j}=\frac{1}{m_s}\mathrm{Im}\left[\psi*\delta(s-s_0)\frac{\partial}{\partial s}\psi\right], \tag{22}$$

$m_s=\mu_N$, $s=R$, $s_0=R_s$ for dissociation, $m_s=\mu_e$, $s=z$, $s_0=z_s$ for ionization. The norm depicted in Fig. 2(a) first drops due to the electronic ionization. After a plateau evolution, it continues to go down owing to dissociation, and the remains stand for the stationary molecular hydrogen ion. It is clear that the probability of ionization is much larger than that of dissociation. Figure 2(b) shows the kinetic-energy spectrum for dissociation by FT, and also the KES for dissociation and Coulomb explosion (CE) with the help of the original "virtual detector" method [32], in which the flux operator is ingeniously utilized. We should note that a "binning" procedure is necessary to derive the kinetic-energy distribution in the molecular case, while the aforesaid "virtual detector" in the example of hydrogen atom detects the total energy of electron in a straight way. Here the kinetic-energy distribution $\frac{dN}{dE}$ stands for the probability per eV. Both the KES for dissociation from the flux operator and from FT appear as a three-

peak structure, and the dominant kinetic-energy releases through dissociation are less than 1.5 eV, while the CE spectrum forms a broad peak between 3.5 and 7.5 eV corresponding to internuclear distances in the charge resonance enhanced ionization (CREI) [33,34] region at $4 \leq R \leq 7.5$. The accurate kinetic-energy spectrum of CE by FT is absent due to the fact that the grid must be expanded to prohibitively large boxes since the ionizing electron can be very far from the nucleus. Although the difficulty can be solved to a certain extent by a wave function splitting technique [35], the computational effort will be much greater than the "virtual detector" method. To assess the validity of the code used in the present quantum calculation, we compare the present result to that shown in Fig. 3 of Ref. [19]. Small differences in KES would be found; however, this can be attributed to the different soft Coulomb potential. In Ref. [19], a modified softcore Coulomb potential with a softening function that depends on the internuclear distance has been introduced and used, while that of the form as in Eq. (18) is employed here. In comparison with the previous works [5,19], we have verified the theoretical methodologies and computational code used in the current study to be definitely correct.

The total CPU time for the above convergent results by the serial version of LZH-DICP is also presented in Table I. It strongly supports that the sine-DVR scheme is much better than the CN scheme as demonstrated in example I; smaller spatial grids and time steps are also necessary to get convergence for the CN scheme. In the parallel version of LZH-DICP, the parallelization of all the matrix operations (matrix diagonalization, matrix-matrix, and matrix-vector multiplications, etc.) is transparent with the OpenMP parallel instrument. Parallelism is easily implemented via OpenMP directives, threads share row iterations according to a predefined chunk size, and a parallel region is spawned explicitly scoping all variables. By distributing all the variables across the available processors, and balancing the number of arithmetic operations within each CPU and communication between neighboring CPUs, the parallel performance of LZH-DICP shall save the CPU time considerably on state-of-the-art supercomputers. For example, we have done a simple scaling test of example III in Table I using an Intel(R) Xeon(R) CPU 2.60 GHz Quad-Core processor. The time cost per step including one iteration for nuclear and M iterations for electron [see Eq. (14)] is illustrated in Fig. 3. We observe a good scaling from serial to parallel execution; almost a factor of 1.5 increase in speed can be reached by doubling the number of CPUs. It should be noted that an approach in which the finite-element DVR is combined with the real-space product algorithm [36] for efficiently solution of the TDSE has been reported recently [37]; parallel treatment of sparse matrices of the splitting kinetic operator with finite difference formula is very intuitive by further splitting and decomposition in one or two dimensions. Although a "superscaling" has been obtained with the message-passing-interface scheme in that work, the sine-DVR scheme presented here appears to compare quite favorably to finite difference methods and, hence, the sine-DVR scheme itself exhibits to be more attractive than the parallelization for the LZH-DICP program.

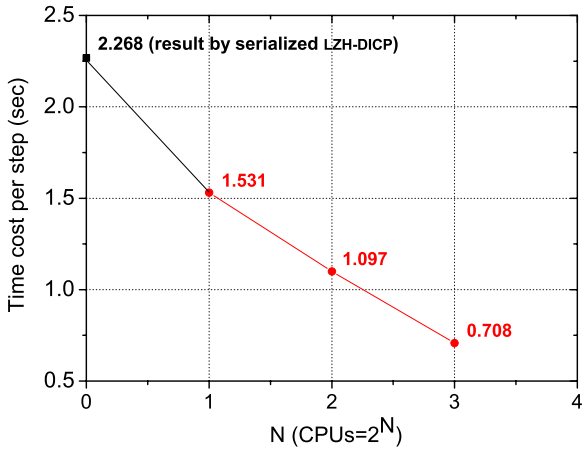

FIG. 3. (Color online) Scaling test results for Ex. III by the LZH-DICP program on Intel(R) Xeon(R) CPU 2.60 GHz Quad-Core processor. A linear scaling is seen from serial to parallel implements.

On account of the validity and the high efficiency of LZH-DICP, its further application to multidimensional treatment is hopeful. Actually, the full 3D calculations for H_2^+ are in progress to solve an underlying disagreement between the experiment and theory, that is, the probability of CE is much smaller than that of dissociation on some experimental conditions [38], while the theoretical conclusion of the 1D model is just contrary to experiment. It was recently shown that the dissociation and ionization depend very sensitively on the softening parameters [21]. The preliminary results of the 3D non-BO treatment incline to the experiment, and more details will be deferred to subsequent work.

IV. CONCLUSIONS

In this paper, we have presented the quantum wave packet theory, especially a proposed sine-DVR scheme, to study the interaction of a laser with atoms and small molecules. Based on these theories, a parallel computer code LZH-DICP has been developed and introduced. Moreover, calculations and comparisons with different methods of both hydrogen atom and molecular hydrogen ion in linearly polarized fields have confirmed the high efficiency of our program, and the parallelization test of the case for molecular hydrogen ion demonstrates a linear scaling on the available computer architecture. In addition, the flux operator is proved to be a powerful tool for analyzing the dynamics. The program which takes the advantages of some techniques allows realistic investigations of the behavior of atoms and small molecules in laser fields. We will exhibit its perspectives by quantitatively simulating recent experimental observables in the future.

ACKNOWLEDGMENTS

R.-F.L. would like to thank B. D. Esry, K. C. Kulander, and K. Bartschat for their helpful advice. This work was supported by the NSFC (Grant No. 20573110).

[1] J. H. Posthumus, Rep. Prog. Phys. **67**, 623 (2004).
[2] P. Agostini and L. F. DiMauro, Rep. Prog. Phys. **67**, 813 (2004).
[3] P. B. Corkum and F. Krausz, Nat. Phys. **3**, 381 (2007); J. Levesque and P. B. Corkum, Can. J. Phys. **84**, 1 (2006); I. Osborne and J. Yeston, Science **317**, 765 (2007); P. H. Bucksbaum, *ibid.* **317**, 766 (2007); E. Goulielmakis, V. S. Yakovlev, A. L. Cavalieri, M. Uiberacker, V. Peryak, A. Apolonski, R. Kienberger, U. Kleineberg, and F. Krausz, *ibid.* **317**, 769 (2007); H. Kapteyn, O. Cohen, I. Christov, and M. Murnane, *ibid.* **317**, 775 (2007).
[4] P. B. Corkum, Phys. Rev. Lett. **71**, 1994 (1993).
[5] X. Chen, A. Sanpera, and K. Burnett, Phys. Rev. A **51**, 4824 (1995).
[6] H. G. Muller, Phys. Rev. A **60**, 1341 (1999).
[7] R. Wiehle, B. Witzel, H. Helm, and E. Cormier, Phys. Rev. A **67**, 063405 (2003).
[8] Z. Chen, T. Morishita, Anh-Thu Le, M. Wickenhauser, X. M. Tong, and C. D. Lin, Phys. Rev. A **74**, 053405 (2006).
[9] S. X. Hu and L. A. Collins, Phys. Rev. Lett. **96**, 073004 (2006).
[10] H. Yu and A. D. Bandrauk, J. Chem. Phys. **102**, 1257 (1995).
[11] L. Y. Peng, D. Dundas, J. F. McCann, K. T. Taylor, and I. D. Williams, J. Phys. B **36**, L295 (2003).
[12] Q.-T. Meng, G.-H. Yang, H.-L. Sun, K.-L. Han, and N.-Q. Lou, Phys. Rev. A **67**, 063202 (2003).
[13] A. Staudte *et al.*, Phys. Rev. Lett. **98**, 073003 (2007).
[14] C. Ruiz, L. Plaja, L. Roso, and A. Becker, Phys. Rev. Lett. **96**, 053001 (2006).
[15] S. Chelkowski, T. Zuo, O. Atabek, and A. D. Bandrauk, Phys. Rev. A **52**, 2977 (1995).
[16] K. C. Kulander, F. H. Mies, and K. J. Schafer, Phys. Rev. A **53**, 2562 (1996).
[17] I. Kawata, H. Kono, and Y. Fujimura, J. Chem. Phys. **110**, 11152 (1999).
[18] W. Qu, Z. Chen, Z. Xu, and C. H. Keitel, Phys. Rev. A **65**, 013402 (2001).
[19] B. Feuerstein and U. Thumm, Phys. Rev. A **67**, 043405 (2003).
[20] B. Feuerstein and U. Thumm, Phys. Rev. A **67**, 063408 (2003).
[21] G. L. Ver Steeg, K. Bartschat, and I. Bray, J. Phys. B **36**, 3325 (2003).
[22] V. Roudnev, B. D. Esry, and I. Ben-Itzhak, Phys. Rev. Lett. **93**, 163601 (2004).
[23] J. Hu, K. L. Han, and G. Z. He, Phys. Rev. Lett. **95**, 123001 (2005); J. Hu, M. S. Wang, K. L. Han, and G. Z. He, Phys. Rev. A **74**, 063417 (2006).
[24] M. Lein, Phys. Rev. Lett. **94**, 053004 (2005).
[25] A. Askar and A. S. Cakmak, J. Chem. Phys. **68**, 2794 (1978).
[26] H. Z. Lu and A. D. Bandrauk, J. Chem. Phys. **115**, 1670 (2001).
[27] O. Sharafeddin and J. Z. H. Zhang, Chem. Phys. Lett. **204**, 190 (1993).
[28] R. F. Lu, T. S. Chu, and K. L. Han, J. Phys. Chem. A **109**, 6683 (2005); T. S. Chu, Y. Zhang, and K. L. Han, Int. Rev. Phys. Chem. **25**, 201 (2006); T. S. Chu, R. F. Lu, K. L. Han, X. N. Tang, H. F. Xu, and C. Y. Ng, J. Chem. Phys. **122**, 244322 (2005); R. F. Lu, T. S. Chu, Y. Zhang, K. L. Han, A. J. C. Varandas, and J. Z. H. Zhang, *ibid.* **125**, 133108 (2006); R. F. Lu, P. Y. Zhang, T. S. Chu, T. X. Xie, and K. L. Han, *ibid.* **126**, 124304 (2007); T. X. Xie, Y. Zhang, M. Y. Zhao, and K. L. Han, Phys. Chem. Chem. Phys. **5**, 2034 (2003).
[29] G. G. Balint-Kurti, R. N. Dixon, and C. C. Marston, J. Chem. Soc., Faraday Trans. **86**, 1741 (1990).
[30] X. M. Tong and S. I. Chu, Phys. Rev. A **57**, 452 (1998).
[31] D. Bauer and P. Koval, Comput. Phys. Commun. **174**, 396 (2006).
[32] B. Feuerstein and U. Thumm, J. Phys. B **36**, 707 (2003).
[33] T. Zuo and A. D. Bandrauk, Phys. Rev. A **52**, R2511 (1995).
[34] T. Seideman, M. Y. Ivanov, and P. B. Corkum, Phys. Rev. Lett. **75**, 2819 (1995).
[35] S. Chelkowski, C. Foisy, and A. D. Bandrauk, Phys. Rev. A **57**, 1176 (1998).
[36] B. I. Schneider and L. A. Collins, J. Non-Cryst. Solids **351**, 1551 (2005).
[37] B. I. Schneider, L. A. Collins, and S. X. Hu, Phys. Rev. E **73**, 036708 (2006).
[38] I. Ben-Itzhak, P. Q. Wang, J. F. Xia, A. M. Sayler, M. A. Smith, K. D. Carnes, and B. D. Esry, Phys. Rev. Lett. **95**, 073002 (2005).